

**Phonon blockade in an acoustic cavity coupled to a three-level artificial atom**Wenzhi Xie, Qin Guo , and Zhenglu Duan *College of Physics, Communication and Electronics, Jiangxi Normal University, Nanchang 330022, China*

(Received 26 October 2021; revised 15 September 2022; accepted 19 September 2022; published 26 September 2022)

We theoretically investigated the phonon statistics of an acoustic cavity coupled to a three-level ladder-type artificial atom. Based on the wave function method, we elucidated the optimal conditions for a strong phonon antibunching effect at zero temperature and observed the coexistence of both conventional and unconventional phonon blockades. Particularly, intersection points occurred between the antibunching structures of both blockades at a certain controlled field strength. Importantly, compared to the conventional/unconventional phonon blockade, simultaneously strong antibunching and high brightness (mean phonon number) were realized at the intersection point. Further, phonon blockade at a finite temperature was studied. We showed that thermal noise affected the phonon blockade only at temperatures exceeding a certain threshold value. More interestingly, the conventional phonon blockade was more robust against thermal noise than the unconventional phonon blockade. Thus, this work provides a scheme for preparing high-quality single-phonon sources at finite temperatures.

DOI: [10.1103/PhysRevB.106.115435](https://doi.org/10.1103/PhysRevB.106.115435)**I. INTRODUCTION**

Single-photon sources are among the important quantum resources used in quantum communication, information processing, and cryptography [1]. They have been prepared using a variety of schemes such as resonant pulsed excitation in quantum dots [2] and the photon blockade effect [3–7]. Photon blockade is a pure quantum phenomenon, in which the strong nonlinearity of an optical cavity prevents more than one photon from entering a cavity. Since it was first proposed, it has been observed in experiments [8–11]. Recently, photon blockade has been extended to multiphoton blockades [12–15] and nonreciprocal cases [16,17], and it also has an acoustical counterpart, which has been termed as phonon blockade [18,19].

As quanta of mechanical vibration, phonons have low traveling velocities and long wavelengths. They can facilitate the integration of acoustic devices with various quantum systems to explore different physical regions [20,21]. Owing to these advantages, they are used as quantum information carriers and show significant potential in the fields of quantum communication and information processing [22–24].

Phonon blockade refers to the phenomenon in which the phonons in mechanical resonators exhibit antibunching behavior. Therefore, using phonon blockade in preparing single-/multiphoton sources [15,25] and other potential single-phonon devices [23,24] is a natural solution. There are two main physical mechanisms of phonon blockade: strong nonlinearity leading to nonuniform energy ladders and quantum interference between the different transition paths of phonons. The former is called conventional phonon blockade (CPNB) [26–38], and the latter is called unconventional phonon blockade (UCPNB) [39–49]. Compared with that of UCPNB, the mean number of phonons (brightness) produced by CPNB is usually larger, but the antibunching (purity) is

poorer. Usually, a strong nonlinearity or coupling strength is the basic condition for CPNB, whereas the converse is required for UCPNB. Owing to the weak intrinsic nonlinearity of a mechanical resonator, CPNB is mainly observed in a composite quantum system, such as a resonator-two-level system [27,28] and an optomechanical system [29–34]. These works about phonon blockade only study either CPNB or UCPNB. Recently, investigations of CPNB and UCPNB in the same system have been reported, among which some works discussed CPNB and UCPNB in different parameter regimes [50,51] and some works studied the overlap of CPB and UCPB in the same parameter regime [52–55].

Thus far, few experimental demonstrations of phonon blockade have been reported [56]. The difficulties in experimentally observing phonon blockade can be listed as follows: First, the CPNB requires strong nonlinearity or strong coupling. However, in most systems, the acoustic nonlinearity is not sufficiently strong. Second, although the UCPNB can occur in a weakly nonlinear regime, the rapid oscillation of the correlation of the generated phonon field [57] and low emission rate can limit observation of the phonon blockade effect. Third, the coherence of phonons is easily destroyed by thermal noise. Only when the phonon energy is greater than or comparable to the thermal energy can the quantum behaviors of the phonons be observed. With the continuous progress in nanomechanical manufacturing technology [58–61], it is possible to cool a mechanical resonator near to its quantum ground state [62,63]. Notwithstanding, the thermal noise in mechanical resonators cannot be eliminated, and phonon blockade is fragile with the presence of thermal noise. However, researchers have found that the CPNB [27–29] is more robust to thermal noise than the UCPNB [41,47]. Hence, explaining the destruction of the antibunching effect of phonons by thermal noise and the preparation of single-phonon sources with better performance at finite temperatures still remains

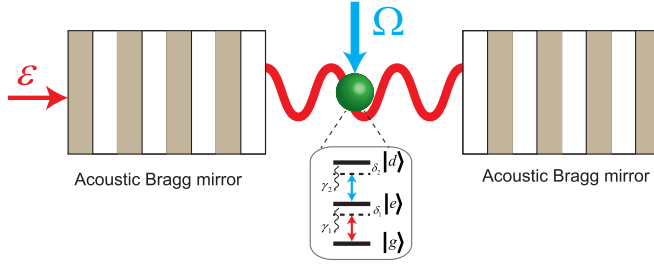


FIG. 1. Sketch of the proposed model. A three-level ladder-type artificial atom is coupled to an acoustic cavity, which consists of a pair of acoustic Bragg mirrors. The  $|g\rangle \leftrightarrow |e\rangle$  transition is driven by the acoustic cavity with an eigenfrequency  $\omega_a$ . The  $|e\rangle \leftrightarrow |d\rangle$  transition is driven by a control field. The acoustic cavity is driven by a weak acoustic field with an eigenfrequency  $\omega_p$ .

challenging. More importantly, a scheme to generate a single phonon that is robust to thermal noise with higher purity and brightness is necessary.

Based on the above-mentioned points, we investigated the phonon blockade effect in a system consisting of a three-level ladder-type artificial atom coupled to an acoustic cavity and a control field at both zero and finite temperatures. Compared with the previous phonon antibunching or blockade schemes, such as the resonator-two-level system [18,27,28], our model has an additional control field to adjust the features of CPNB and UCPNB to observe more complicated phonon blockade effect. We found that CPNB and UCPNB coexisted in this system for strong coupling strength with suitable control field strength. Moreover, similar to the photonic counterpart in Refs. [52–55], they intersected, resulting in a generated phonon field with both the advantages of a strong antibunching effect and a relatively large mean phonon number. Therefore, in this work we can combine the advantages of both CPNB and UCPNB. It is a key innovation of this work. This offers an opportunity for experimental realization of a single phonon with higher quality and also enabled us to further understand the physical mechanism governing them. In addition, as a phononic field is fragile to thermal noise, we carefully study the influence of temperature on the properties of the phononic field at the intersection point of CPNB and UCPNB in our work, which is absent in the previous works [52–55]. Our results facilitate the preparation of high-quality single-phonon sources at finite temperature, providing potential applications for on-chip quantum communication and information processing.

The remainder of this paper is organized as follows. In Sec. II, we describe the proposed model. In Sec. III, we derive the optimal conditions for CPNB and UCPNB based on the wave function method. In Sec. IV, we numerically discuss the correlation function and the average phonon number of the phonon field at zero and finite temperatures. Finally, we conclude this paper in Sec. V.

## II. MODEL

Figure 1 presents our proposed model, where a three-level ladder-type artificial atom is embedded in an acoustic cavity consisting of two Bragg acoustic mirrors. The artificial atom

can be a tunable gap superconducting flux qubit [64] or a transmon-type superconducting circuit [65,66]. The energy levels of the artificial atom are labeled as  $|g\rangle$ ,  $|e\rangle$ , and  $|d\rangle$ . The acoustic cavity is directly coupled to the  $|g\rangle \leftrightarrow |e\rangle$  transition. It is driven by a weak external acoustic driving field with frequency  $\omega_p$  and amplitude  $\varepsilon$ . A strong control field with frequency  $\omega_q$  and amplitude  $\Omega$  is directly coupled to the  $|e\rangle \leftrightarrow |d\rangle$  transition in a direction perpendicular to the cavity axis. The control field can be an acoustic field [64] or microwave field [65]. In the rotating-wave approximation frame of the weak driving field and strong control field defined by  $U(t) = \exp[-i(\omega_p(\hat{a}^\dagger \hat{a} + \hat{\sigma}_{ee}) + \omega_q \hat{\sigma}_{dd})t]$ , the Hamiltonian can be written as ( $\hbar = 1$ ),

$$\hat{H} = \Delta \hat{a}^\dagger \hat{a} + \delta_1 \hat{\sigma}_{ee} + \delta_2 \hat{\sigma}_{dd} + g(\hat{a} \hat{\sigma}_{eg} + \hat{a}^\dagger \hat{\sigma}_{ge}) + \Omega(\hat{\sigma}_{ed} + \hat{\sigma}_{de}) + \varepsilon(\hat{a} + \hat{a}^\dagger), \quad (1)$$

where  $\hat{a}(\hat{a}^\dagger)$  is the annihilation (creation) operator of the phonon mode in the acoustic cavity with the fundamental mode frequency  $\omega_a$ .  $\hat{\sigma}_{j,k} = |j\rangle\langle k|$  is the transition operator for the atomic states with  $\{j, k\} = \{g, e, d\}$ .  $\omega_e$  and  $\omega_d$  are the eigenfrequencies of the first excited state  $|e\rangle$  and the second excited state  $|d\rangle$ , respectively.  $g$  is the phonon-atom coupling strength.  $\Delta = \omega_a - \omega_p$  is the detuning between the acoustic cavity and the weak driving field.  $\delta_1 = \omega_e - \omega_p$  and  $\delta_2 = \omega_d - \omega_p$  are atomic detunings.

With the inclusion of the acoustic cavity decay  $\kappa$  and atomic spontaneous emission rates  $\gamma_1$  from  $|d\rangle$  to  $|e\rangle$  ( $\gamma_2$  from  $|e\rangle$  to  $|g\rangle$ ) states, we can express the non-Hermitian effective Hamiltonian as

$$\hat{H}_{\text{eff}} = \Delta' \hat{a}^\dagger \hat{a} + \delta'_1 \hat{\sigma}_{ee} + \delta'_2 \hat{\sigma}_{dd} + g(\hat{a} \hat{\sigma}_{eg} + \hat{a}^\dagger \hat{\sigma}_{ge}) + \Omega(\hat{\sigma}_{ed} + \hat{\sigma}_{de}) + \varepsilon(\hat{a} + \hat{a}^\dagger), \quad (2)$$

where the effective detunings are  $\Delta' = \Delta - i\kappa/2$ ,  $\delta'_1 = \delta_1 - i\gamma_1/2$ , and  $\delta'_2 = \delta_2 - i\gamma_2/2$ . In fact, Eq. (2) describes electromagnetically induced acoustic transparency [66].

## III. PHONON BLOCKADE CONDITION

In this section, we first derive approximate analytical expressions for the second-order correlation function at zero temperature to study the statistical properties of the phonons in the system. Under the condition  $\{\varepsilon, \gamma\} \ll \kappa \ll \Omega$ , high-phonon excitation states have very low populations, and the state of the system in the few-phonon subspace can be described by

$$|\psi\rangle = C_{0,g}|0, g\rangle + C_{1,g}|1, g\rangle + C_{0,e}|0, e\rangle + C_{0,d}|0, d\rangle + C_{2,g}|2, g\rangle + C_{1,e}|1, e\rangle + C_{1,d}|1, d\rangle, \quad (3)$$

where the coefficient  $C_{n,m}$  is the probability amplitude of the state  $|n, m\rangle$  with  $n$  phonons ( $n = 0, 1, 2, \dots$ ) and the atomic state  $|m\rangle$  ( $m = g, e, d$ ). By substituting the effective Hamiltonian Eq. (2) and wave function Eq. (3) into the Schrödinger equation,  $i\partial|\psi\rangle/\partial t = \hat{H}_{\text{eff}}|\psi\rangle$  [67]. By considering  $\{C_{0,g} \simeq 1\} \gg \{C_{1,g}, C_{0,e}, C_{0,d}\} \gg \{C_{2,g}, C_{1,e}, C_{1,d}\}$ , a set of coefficient equations can be obtained as follows:

$$i\dot{C}_{1,g} = \Delta' C_{1,g} + gC_{0,e} + \varepsilon C_{0,g}, \quad (4)$$

$$i\dot{C}_{0,e} = \delta'_1 C_{0,e} + gC_{1,g} + \Omega C_{0,d}, \quad (5)$$

$$i\dot{C}_{0,d} = \delta'_2 C_{0,d} + \Omega C_{0,e}, \quad (6)$$

$$i\dot{C}_{2,g} = 2\Delta' C_{2,g} + \sqrt{2}gC_{1,e} + \sqrt{2}\varepsilon C_{1,g}, \quad (7)$$

$$i\dot{C}_{1,e} = (\Delta' + \delta'_1)C_{1,e} + \sqrt{2}gC_{2,g} + \Omega C_{1,d} + \varepsilon C_{0,e}, \quad (8)$$

$$i\dot{C}_{1,d} = (\Delta' + \delta'_2)C_{1,d} + \Omega C_{1,e} + \varepsilon C_{0,d}. \quad (9)$$

By setting  $\partial C_{n,m}/\partial t = 0$ , we obtain steady-state solutions for the coefficients  $C_{1,g}$  and  $C_{2,g}$ :

$$C_{1,g} = -\frac{\delta'_1 \delta'_2 - \Omega^2}{\Delta' C - \delta'_2 g^2} \varepsilon, \quad (10)$$

$$C_{2,g} = \frac{g^2(\delta'_2 + A) + C(B - A)}{\sqrt{2}(\Delta' C - \delta'_2 g^2)(\Delta'(B - A) - g^2)} \varepsilon^2, \quad (11)$$

$$C_{2,g} = \frac{g^2(\delta'_2 B + \Omega^2) + C(B^2 - \Omega^2)}{\sqrt{2}(\Delta' C - \delta'_2 g^2)(\Delta'(B^2 - \Omega^2) - Bg^2)},$$

where  $A = \Omega^2/(\Delta' + \delta'_2)$ ,  $B = \Delta' + \delta'_1$ , and  $C = \delta'_1 \delta'_2 - \Omega^2$ . In the following section, we consider only the simple cases:  $\delta_1 = \delta_2 = \delta$  and  $\gamma_1 = \gamma_2 = \gamma$ .

The approximate solution of the second-order correlation function is expressed as

$$g^{(2)}(0) = \frac{\langle \Psi | \langle \hat{a}^\dagger \hat{a}^\dagger \hat{a} \hat{a} \rangle | \Psi \rangle}{\langle \Psi | \langle \hat{a}^\dagger \hat{a} \rangle | \Psi \rangle^2} \approx \frac{2|C_{2,g}|^2}{|C_{1,g}|^4}. \quad (12)$$

From Eq. (12), mathematically, when  $\Delta'(\delta'^2 - \Omega^2) - \delta'g^2 = 0$  or  $g^2[\delta'(\Delta' + \delta') + \Omega^2] + [(\Delta' + \delta')^2 - \Omega^2](\delta^2 - \Omega^2) = 0$ , the second-order correlation function  $g^{(2)}(0)$  will be zero. In the following we discuss both cases.

(i)  $\Delta'(\delta'^2 - \Omega^2) - \delta'g^2 = 0$ . The optimal condition can be decomposed into real and imaginary components:

$$g^2\delta + \Delta(\Omega^2 - \delta^2) + (\Delta\gamma + 2\kappa\delta)\gamma/4 = 0, \quad (13)$$

$$((g^2 - 2\Delta\delta)\gamma + \kappa(\Omega^2 - \delta^2) + \kappa\gamma^2/4)/2 = 0. \quad (14)$$

We can see that, in the limit of strong coupling, that is,  $g \gg \{\kappa, \gamma\}$ , the imaginary part (the order of  $\{\kappa, \gamma\}$ ) is much less than the real part (the order of  $g$ ). Therefore, under this assumption, the optimal condition  $\Delta'(\delta'^2 - \Omega^2) - \delta'g^2 = 0$  can be reduced to

$$g^2\delta + \Delta(\Omega^2 - \delta^2) \simeq 0. \quad (15)$$

To confirm the validity of the above approximation, we present the absolute value of  $\Delta'(\delta'^2 - \Omega^2) - \delta'g^2$  and its real and imaginary parts in Fig. 2(a). It is seen that, compared to the real part, the imaginary part is too small to have influence on the optimal condition. Thus, the real part itself can serve as the optimal condition. Besides, from Fig. 2(a) we know that Eq. (15) can determine the local minimized values of the second-order correlation function, as shown by the black vertical dashed lines. Equation (10) reveals that, when the condition [Eq. (15)] holds, the single phonon state's population will be resonantly enhanced. This is a typical feature of CPNB, similar to the photonic counterpart [68]. This is because an anharmonic level of a quantum phononic system induced by strong coupling between phonons prevents the population of two-/multiphonon states [69]. Therefore, the

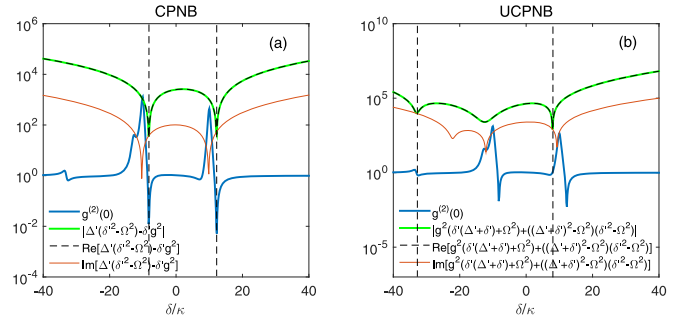


FIG. 2. Comparison between the optimal conditions and their real and imaginary parts for the case of (a) CPNB and (b) UCPNB, and second-order correlation function  $g^{(2)}(0)$  with fixed  $\Delta = 25\kappa$ ,  $\Omega = 10\kappa$ . The positions of best CPNB/UCPNB are indicated by the black vertical dashed lines. The other parameters are taken as  $g = 10\kappa$ ,  $\varepsilon = 0.01\kappa$ , and  $\gamma = 0.01\kappa$ .

optimal condition [Eq. (15)] contributes toward CPNB. We further observe that, without a control field, that is,  $\Omega = 0$ , the optimal condition reduces to  $g^2 - \Delta\delta = 0$ , which is similar to the optimal condition for the phonon blockade in a mechanical resonator coupled to a two-level system [27]. Here, we must stress that, in a weak coupling regime, although the optimal conditions [Eq. (15)] can be satisfied, the anharmonicity of a level structure is extremely small. Hence, two- and multiphonon states can be resonantly excited as a single-phonon state, which hinders the occurrence of the phonon blockade.

(ii)  $g^2[\delta'(\Delta' + \delta') + \Omega^2] + [(\Delta' + \delta')^2 - \Omega^2](\delta^2 - \Omega^2) = 0$ . This equation is perfectly satisfied within the limit of weak coupling. However, we investigate the scenario of the coexistence of both CPNB and UCPNB. Hence, we only consider the case of the limit of strong coupling, that is,  $g \gg \{\kappa, \gamma\}$ . Under this condition, we can obtain the real and imaginary parts of the optimal condition as follows:

$$g^2(\Omega^2 + \delta^2 + \Delta\delta) - (\Omega^2 - \delta^2)[(\Delta + \delta)^2 - \Omega^2] \simeq 0, \quad (16)$$

$$\gamma(\Delta + 2\delta) \left[ \Omega^2 - \frac{g^2}{2} - \delta(\Delta + \delta) \right] + \kappa \left[ (\Delta + \delta)(\Omega^2 - \delta^2) - \frac{1}{2}\delta g^2 \right] \simeq 0. \quad (17)$$

Similarly, the imaginary part is much less than the real part in the strong coupling limit. Therefore, we can approximately use the real part of the optimal condition to determine the optimal parameters for best antibunching effect. Figure 2(b) shows that the curve of the real part [Eq. (16)] overlaps the absolute value of the optimal condition and its dips exactly correspond to the dips of the second-order correlation function whose values are considerably less than 1. Particularly, the condition [Eq. (16)] minimizes the population for the two-phonon state, while the populations of the other states do not undergo significant changes. This is a typical feature of UPNB. Physics leading to the UCPNB effect is the destructive quantum interference of the two-phonon state between different phonon transition pathways. Contrary to the perfect destructive quantum interference in a weak coupling regime, the condition [Eq. (16)] leads to imperfect quantum

interference. Here we should stress that, due to the non-Hermitian effective Hamiltonian excluding the thermal excitation, the optimal conditions [Eqs. (15) and (16)] are merely suitable for the case of zero temperature.

#### IV. NUMERICAL SIMULATION AND ANALYSIS

As stated in Ref. [70], the non-Hermitian effective Hamiltonian may lead to a different result from that based on full quantum treatment on an open quantum system. To verify the analytical results presented in the previous section and further investigate the effect of thermal noise on the quantum statistics of the phononic field, we use the quantum master equation to simulate the dynamics of the system:

$$\begin{aligned} \dot{\rho} = & -i[\hat{H}, \rho] + \frac{\gamma_1}{2}(2\sigma_{ge}\rho\hat{\sigma}_{eg} - \hat{\sigma}_{eg}\hat{\sigma}_{ge}\rho - \rho\hat{\sigma}_{eg}\hat{\sigma}_{ge}) \\ & + \frac{\gamma_2}{2}(2\hat{\sigma}_{ed}\rho\hat{\sigma}_{de} - \hat{\sigma}_{de}\hat{\sigma}_{ed}\rho - \rho\hat{\sigma}_{de}\hat{\sigma}_{ed}) \\ & + \frac{\kappa}{2}(n_{th} + 1)(2\hat{a}\rho\hat{a}^\dagger - \hat{a}^\dagger\hat{a}\rho - \rho\hat{a}^\dagger\hat{a}) \\ & + \frac{\kappa}{2}n_{th}(2\hat{a}^\dagger\rho\hat{a} - \hat{a}\hat{a}^\dagger\rho - \rho\hat{a}\hat{a}^\dagger), \end{aligned} \quad (18)$$

where  $\rho$  is the density matrix of the phonon-atom system. The thermal mean phonon number  $n_{th} = [\exp(T_0/T) - 1]^{-1}$ , where  $T$  is the environmental temperature and  $T_0 = \hbar\omega_a/k_B$  is the characteristic temperature of the system with the Boltzmann constant  $k_B$ . In the infinite-time limit, the second-order correlation function for the steady state is given by

$$g^{(2)}(0) = \frac{\text{Tr}(\hat{a}^\dagger\hat{a}^\dagger\hat{a}\hat{a}\rho)}{\text{Tr}(\hat{a}^\dagger\hat{a}\rho)^2}, \quad (19)$$

and the mean phonon number is

$$\langle N \rangle = \text{Tr}(\hat{a}^\dagger\hat{a}\rho). \quad (20)$$

##### A. Zero Temperature

We first consider the case at zero temperature when the system is in a strong-coupling regime, that is,  $g \gg (\gamma, \kappa)$ . Here we consider  $g = 10\gamma$  and  $\gamma = \kappa/100$  [71] as an example. In Fig. 3(a), we present  $g^{(2)}(0)$  as a function of cavity detuning  $\Delta$  and atomic detuning  $\delta$  based on the numerical simulation with Eqs. (18) and (19). Moreover, a strong phonon antibunching structure is observed [dark blue region indicates  $g^{(2)}(0) \ll 1$ ]. This implies that a strong phonon blockade exists in our model. To distinguish the type of phonon antibunching structure, we plotted the optimal conditions for CPNB [Eq. (15)] with green dashed lines and those for UCPNB [Eq. (16)] with black dashed lines, as shown in Fig. 3(a). Further, the curves for the optimal conditions [Eqs. (15) and (16)] perfectly match the numerical results, which implies that CPNB and UCPNB coexist in this situation. Interestingly, we found two intersection points (labeled A and B) between them, where both their advantages could be retained.

We also numerically evaluated the mean phonon number in Fig. 3(b). Compared with Fig. 3(a), we found that the structure of the maximum value of the mean phonon number was similar to that of the CPNB. To explain the numerical results,

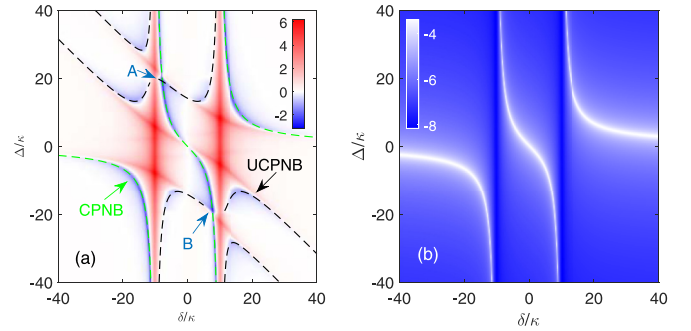


FIG. 3. (a) Second-order correlation function  $g^{(2)}(0)$  (logarithmic scale) as a function of atomic detuning  $\delta$  and cavity detuning  $\Delta$ . The green dashed lines represent the optimal condition to CPNB given by Eq. (15) and the black dashed lines represent the optimal condition to UCPNB given by Eq. (16). (b) Mean phonon number (logarithmic scale) as a function of atomic detuning  $\delta$  and cavity detuning  $\Delta$ . Other parameters are taken as  $g = 10\kappa$ ,  $\varepsilon = 0.01\kappa$ ,  $\Omega = 10\kappa$ , and  $\gamma = 0.01\kappa$ .

we derived the expression of the mean phonon number:

$$\begin{aligned} \langle \hat{N} \rangle & \simeq |C_{1,g}|^2 \\ & = \left| \frac{(\delta'^2 - \Omega^2)\varepsilon}{\Delta'(\delta'^2 - \Omega^2) - \delta'g^2} \right|^2. \end{aligned} \quad (21)$$

Notably, when the optimal condition for CPNB [Eq. (15)] holds, the mean phonon number [Eq. (21)] is resonantly enhanced, which is a typical characteristic of CPNB.

To verify the validity of the approximate analytical analyses based on the non-Hermitian Hamiltonian [Eq. (2)], we plotted the second-order correlation function and mean phonon number using both approximate analytical results and exact numerical results in Fig. 4. We can see that, for the case of a weak control field, i.e.,  $\Omega = 0.001\kappa$ , the analytical results are consistent with the numerical ones. With increasing the control field strength, the analytical results gradually deviate from the numerical results. In spite of this deviation, the positions for the minimal values of the second-order correlation functions on the analytical curves agree well with those on numerical curves. In other words, the analytical optimal conditions [Eqs. (15) and (16)] are valid.

To thoroughly investigate the properties of the phononic field at intersection point A, we plotted the second-order and higher-order correlation functions and the mean phonon number  $\langle \hat{N} \rangle$  as a function of  $\delta$  around point A in Figs. 5(a)– 5(c). Here the  $n$ th-order equal-time correlation function is defined as  $g^{(n)}(0) = \text{Tr}(\hat{a}^{\dagger n}\hat{a}^n\rho)/\text{Tr}(\hat{a}^\dagger\hat{a}\rho)^n$  ( $n = 2, 3, \dots$ ) [53,72]. Figures 4(a) and 4(b) describe  $g^{(2)}(0)$ ,  $g^{(3)}(0)$ , and  $g^{(4)}(0)$  when the parameters satisfy the optimal conditions for CPNB and UCPNB, respectively, which corresponds to the green (black) arrow in Fig. 3(a). In particular, when  $\delta \simeq -7.7\kappa$ , which corresponds to the intersection point, a sharp and deep dip occurs on the curve of the correlation function for both CPNB and UCPNB cases. From Fig. 5(a), it is seen that  $1 \gg g^{(2)}(0) \gg g^{(3)}(0) \gg g^{(4)}(0)$  under the optimal condition of CPNB in the entire parameter region; however, for the UCPNB case,  $1 \gg g^{(2)}(0) \gg g^{(3)}(0) \gg g^{(4)}(0)$  only holds for the intersection point and its vicinity, while in the

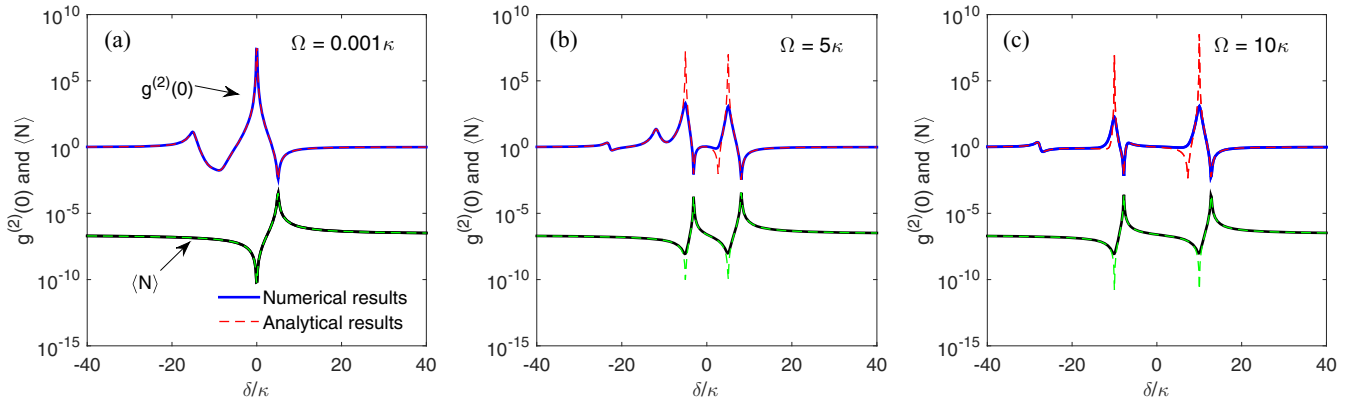


FIG. 4. Second-order correlation function  $g^{(2)}(0)$  and mean phonon number as a function of atomic detuning  $\delta$  with fixed  $\Delta = 20\kappa$  for different control field strengths: (a)  $\Omega = 0.001\kappa$ ; (b)  $\Omega = 5\kappa$ ; and (c)  $\Omega = 10\kappa$ . The dashed lines are given by Eq. (12) and  $\langle N \rangle = |C_{1,g}|^2$ , respectively. Other parameters are taken as  $g = 10\kappa$ ,  $\varepsilon = 0.01\kappa$ , and  $\gamma = 0.01\kappa$ .

region far away from the intersection point the correlation function satisfies the relation  $g^{(3)}(0) > g^{(4)}(0) > 1 > g^{(2)}(0)$ . This means the phononic field at the intersection point has the feature of CPNB rather than that of UCPNB. In particular, the value of the second-order correlation function at the dip on the curve of the CPNB is the smallest one in the parameter region shown in Fig. 5(a). Therefore, the phonon blockade is enhanced at the intersection point. On the other hand, the mean phonon number of UCPNB is resonantly enhanced at the intersection point, and the maximum value equals that of the CPNB, as shown in Fig. 5(c). Based on the above discussion, we can conclude that it is possible to produce a single phonon with the advantages of both the high purity (phonon antibunching) of CPNB and the high brightness (mean phonon number) of UCPNB. To further explore the antibunching feature of the phonon field at intersection point A, we calculated the time-delayed second-order correlation function using the quantum regression theorem  $g^{(2)}(\tau) = \text{Tr} \{ \hat{a}^\dagger \hat{a} e^{\hat{L}\tau} [\hat{a} \hat{\rho}_{ss} \hat{a}^\dagger] \} / \text{Tr} (\hat{a}^\dagger \hat{a} \hat{\rho}_{ss})^2$  [73]. The numerical result of  $g^{(2)}(\tau)$  is plotted in Fig. 5(d) and it is seen that  $g^{(2)}(0) \ll 1$  and  $g^{(2)}(0) < g^{(2)}(\tau)$ . As discussed in Ref. [72],  $1 \gg g^{(2)}(0) \gg g^{(3)}(0) \gg g^{(4)}(0)$  means that the higher-order phonon-number probabilities ( $n = 2, 3, \dots$ ) can be safely ignored and it is an important index for a high-quality single-phonon source. This

indicates that the phononic field at the intersection point is in a high-quality single-phonon state and can serve as a high-quality single-phonon source.

As shown in Fig. 6, we also investigated the effect of the coupling strength  $g$  and the controlled field strength  $\Omega$  on the correlation function  $g^{(2)}(0)$  and the mean phonon number  $\langle \hat{N} \rangle$  at intersection point A. Figure 6(a) shows that the value of the second-order correlation function  $g^{(2)}(0)$  decreases while the mean phonon number slightly increases as  $g$  increases. This indicates that strong coupling is beneficial for phonon blockade. Similarly, the strong control strength  $\Omega$  leads to a stronger phonon antibunching effect, as shown in Fig. 6(b).

To more intuitively demonstrate the effect of the control field on the correlation function of the phonon field in Fig. 7, we plot the images of the second-order correlation function of the phonon field  $g^{(2)}(0)$  as a function of  $\Delta$  and  $\delta$ , with  $\Omega = 5\kappa, 10\kappa$ , and  $15\kappa$ , respectively. At  $\Omega = 5\kappa$ , the intersection of CPNB and UCPNB is noticeable. However, it disappears when  $\Omega = 15\kappa$ . Moreover, the intersection point gradually disappears as the intensity of the control field increases. In addition, two antibunching structures, symmetrically distributed about the zero atomic detuning, occur when the control field exists. The distance between the two centers of the

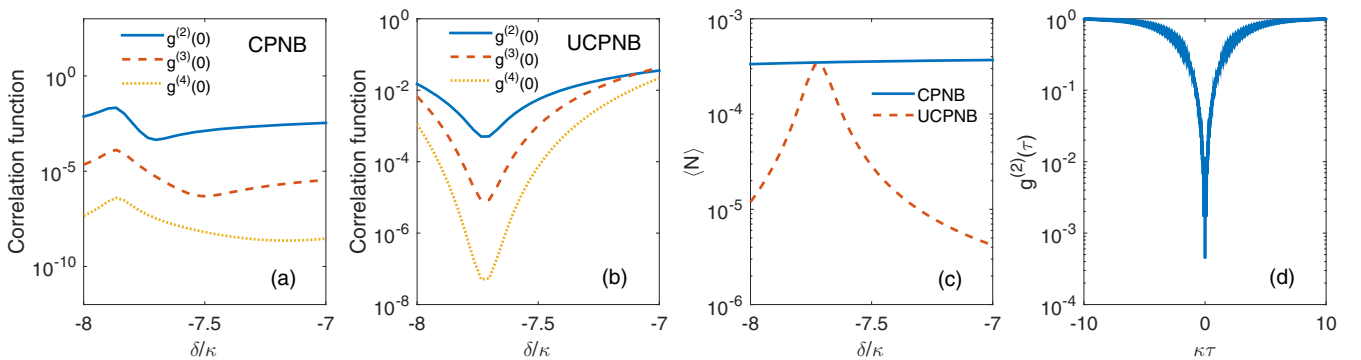


FIG. 5. The correlation functions as a function of atomic detuning  $\delta$  for (a) CPNB with the optimal conditions in Eq. (15) and (b) UCPNB with the optimal condition in Eq. (16) hold. (c) Corresponding mean phonon number for CPNB and UCPNB when optimal conditions [Eqs. (15) and (16)] hold. (d) The time-delayed second-order correlation function for  $\delta = -7.7\kappa$  and other parameters satisfy the optimal condition in Eq. (15). Other parameters are taken as  $g = 10\kappa$ ,  $\varepsilon = 0.01\kappa$ , and  $\gamma = 0.01\kappa$ .

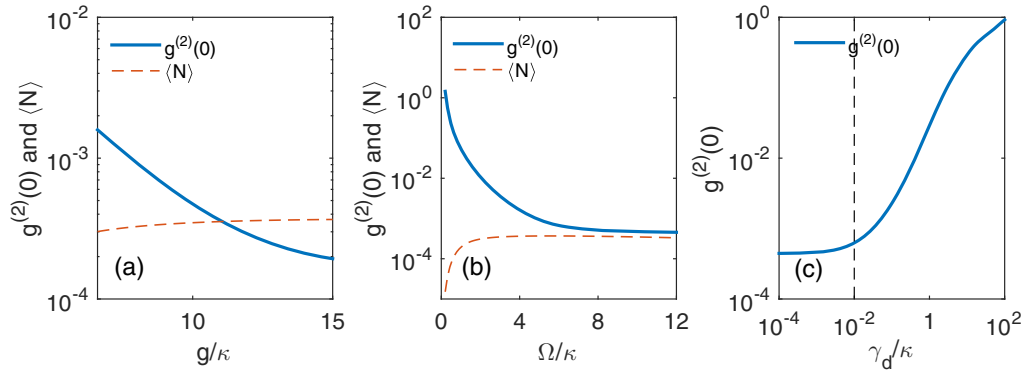


FIG. 6. Second-order correlation function  $g^{(2)}(0)$  and mean phonon number  $\langle N \rangle$  as a function of (a) phonon-atom coupling strength  $g$  with  $\Omega = 10\kappa$  and (b) control field strength  $\Omega$  with  $g = 10\kappa$ . The values of atomic and cavity detunings locate at intersection point A. (c) Second-order correlation function  $g^{(2)}(0)$  as a function of the pure dephasing rate with fixed  $g = 10\kappa$  and  $\Omega = 10\kappa$ . The black dashed line denotes the position of atomic decay rate  $\gamma$ . Other parameters are taken as  $\varepsilon = 0.01\kappa$  and  $\gamma = 0.01\kappa$ .

antibunching structures is equal to  $2\Omega$ . When the control field is small, the two antibunching structures overlap, resulting in an intersection between CPNB and UCPNB. When the control field becomes stronger, the intersection points shift to the weak antibunching region and finally disappear. Further, under the action of the strong control field, the excited state  $|e\rangle$  splits into  $|e_{\pm}\rangle$ , with the energy level shift  $\delta\omega_{\pm} = \pm\Omega$  owing to the Autler-Townes splitting [74]. Moreover, the transition  $|g\rangle \leftrightarrow |e\rangle$  in the bare atomic state becomes  $|g\rangle \leftrightarrow |e_{\pm}\rangle$  in the dressed states. In this situation, we can regard our system, with a strong control field, as two independent J-C-like phononic systems. With suitable control field strength, the CPNB and UCPNB structures of two independent J-C-like models can overlap in the parameter space.

As mentioned in Ref. [5], pure dephasing can affect the degree of antibunching of the photonic mode and degrade the quality of a single-photon source. Thus, we should investigate the effect of pure dephasing on the coherence of the phononic field. We add the Lindblad terms  $L_d[\hat{A}] = \frac{\gamma_d}{2}[2\hat{A}^\dagger\hat{A}\rho\hat{A}^\dagger\hat{A} - (\hat{A}^\dagger\hat{A})^2\rho - \rho(\hat{A}^\dagger\hat{A})^2]$  with  $\hat{A} = \sigma_{ge}(\sigma_{ed})$  to describe the pure dephasing of the three-level artificial atom in the quantum master equation [18]. For simplicity, we have assumed the same dephasing rate  $\gamma_d$  for energy levels  $|e\rangle$  and  $|d\rangle$ . We plot the second-order correlation function of the phonon field versus the pure dephasing rate  $\gamma_d$  in Fig. 6. It is seen that,

when the pure dephasing rate is smaller than the spontaneous emission rate of the artificial atom, i.e.,  $\gamma_d < \gamma$ ,  $g^{(2)}(0)$  almost remains a constant with varying  $\gamma_d$ . It indicates that the pure dephasing does not weaken the phononic antibunching. On increasing the pure dephasing rate, the antibunching is progressively reduced, and finally the system behaves as a coherent acoustic source. We can conclude that our conclusions hold under the condition of low dephasing rate, i.e.,  $\gamma_d < \gamma$ .

## B. Finite temperature

Contrary to a photonic system, a phononic system has a lower eigenfrequency and is more sensitive to thermal noise. However, it is difficult to experimentally cool the mechanical resonator to zero temperature. Therefore, it is necessary to study the phonon blockade at finite temperature. In Fig. 8(a), we plot  $g^{(2)}(0)$  as a function of the environmental temperature  $T$  for both CPNB and UCPNB. Here, we set a fixed atomic detuning  $\delta = -10\kappa$ , and the cavity detuning is determined by the optimal conditions [Eqs. (15) and (16)]. Notably, for CPNB in the temperature region  $[0, 0.07T_0]$ ,  $g^{(2)}(0)$  is a small constant value, which is significantly less than 1. This implies a strong antibunching effect in this region and that the quantum coherence of the phonon field is well maintained in this region. We can conclude that thermal noise

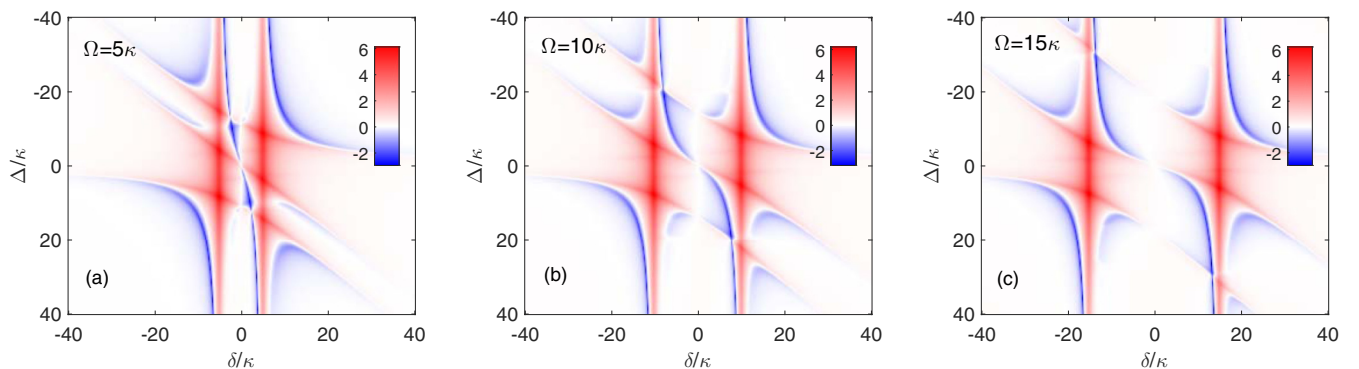


FIG. 7. Second-order correlation function  $g^{(2)}(0)$  (logarithmic scale) as a function of atomic detuning  $\delta$  and cavity detuning  $\Delta$  for different coupling strength: (a)  $\Omega = 5\kappa$ ; (b)  $\Omega = 10\kappa$ ; and (c)  $\Omega = 15\kappa$ . Other parameters are taken as  $g = 10\kappa$ ,  $\varepsilon = 0.01\kappa$ , and  $\gamma = 0.01\kappa$ .

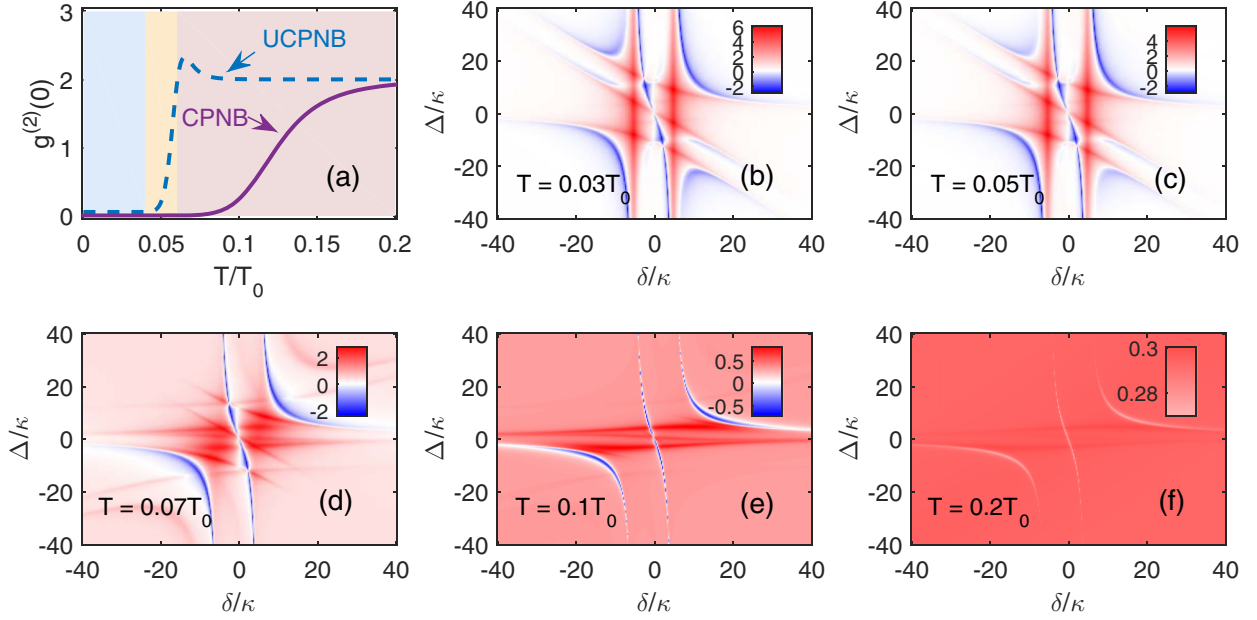


FIG. 8. (a) Second-order correlation function  $g^{(2)}(0)$  vs temperature  $T$  with a fixed atomic detuning of  $\delta = -10\kappa$  and the cavity detuning satisfying the optimal conditions [Eqs. (15) and (16)]. (b) Second-order correlation function  $g^{(2)}(0)$  (logarithmic scale) as a function of atomic detuning  $\delta$  and cavity detuning  $\Delta$  for different temperatures  $T$ .  $\Omega = 10\kappa$ . Other parameters are taken as  $g = 10\kappa$ ,  $\varepsilon = 0.01\kappa$ , and  $\gamma = 0.01\kappa$ .

cannot affect the coherence of a quantum phonon system at a very low temperature for the CPNB. With an increase in the bath temperature and when the threshold value  $0.07T_0$  is exceeded,  $g^{(2)}(0)$  increases rapidly, and the phonon field changes from strong antibunching to bunching. Eventually,  $g^{(2)}(0)$  approaches a constant 2. In other words, the system finally reaches a thermal state and completely loses the quantum coherence. Hence, we can say that thermal noise at high temperatures destroys the quantum coherence of the phonon field. Concerning UCPNB, the behavior of the second-order correlation function is similar to that of CPNB. However, there are several different aspects. First, the temperature range  $[0, 0.04T_0]$  for the quantum coherence preserved is smaller than that in CPNB. In other words, the threshold value for UCPNB is lower than that for CPNB. Second, the transition of the phonon field from strong antibunching to a thermal state is faster than in CPNB. Moreover, in the region  $[0.06T_0, 0.07T_0]$ , the quantum coherence is completely preserved in CPNB, while the phonon state in UCPNB is the thermal state. Therefore, CPNB is more robust against the disturbance of thermal noise than UCPNB.

To better demonstrate the effect of thermal noise on CPNB and UCPNB, we plot the second-order correlation function at different temperatures:  $T = 0.03T_0$ ,  $0.05T_0$ ,  $0.07T_0$ ,  $0.1T_0$ , and  $0.2T_0$ ; this is shown in Figs. 8(b)–8(f). Based on a comparison with the zero-temperature case [as shown in Fig. 8(a)], when  $T = 0.03T_0$ , the suppression of phonon antibunching by thermal noise is not evident; thus, both CPNB and UCPNB are well preserved in our system. At  $T = 0.05T_0$ , the antibunching structure for UCPNB becomes unclear, whereas that for CPNB still remains unchanged. When the temperature increases to  $0.07T_0$ , the antibunching structure for UCPNB completely disappears, whereas the strong antibunching structure for CPNB is unchanged. With a further increase in temperature, for example, at  $T = 0.1T_0$ , the strong antibunch-

ing structure for CPNB is weakened. Moreover, at  $T = 0.2T_0$ , the antibunching structure completely disappears.

*Remark.* To construct a practical single-phonon source based on the scheme discussed in this work, the properties of the output phononic field of the phononic cavity should be evaluated. According to the input-output relation of an open quantum system [75], the output phonon field is given by  $\hat{a}_{\text{out}} = \sqrt{\kappa_{\text{out}}}\hat{a} + \hat{a}_{\text{input}}$  with the output coupling strength  $\kappa_{\text{out}}$  between the phonon cavity and the reservoir and  $\hat{a}_{\text{input}}$  is the input field, which is assumed to be a vacuum. Therefore, the quantum statistics of the output phononic field is the same as that of the intracavity phonon field. If the system is operated at the intersection point of CPNB and UCPNB, we can obtain a high-quality single-phonon source. Additionally, to measure the second-order correlation function of the phononic field generated by our system, one can adopt indirect measurement methods, such as coupling the phonons to an optical system [15,26,76,77].

## V. CONCLUSION

We proposed a feasible scheme to realize a strong phonon blockade by coupling a three-level artificial atom with an acoustic cavity and a coupling field. The optimal parameter conditions for CPNB and UCPNB were analytically presented based on the wave function method and verified by numerical results based on the master equation. We found that CPNB and UCPNB can be realized in a current quantum phononic system. More interestingly, they can coexist at certain parameter values, and these intersection points gradually disappeared with the increasing amplitude of the coupling field. At the intersection point, the second-order correlation function of the phonon field was the same as that of UCPNB, and the mean phonon number was the same as that of CPNB at ordinary points. Therefore, we leveraged both the advantages

of the strong phonon antibunching effect in UCPNB and the relatively large phonon number in CPNB to realize a higher-quality single-phonon state. Finally, the effect of thermal noise on the phonon blockade was investigated. It was found that thermal noise could not affect phonon antibunching until the temperature exceeded a certain threshold value and that CPNB was more insensitive to thermal noise than UCPNB.

## ACKNOWLEDGMENTS

This work is partly supported by the National Natural Science Foundation of China (NSFC) (Grants No. 11964014, No. 11664014, and No. 12064018), the Major Discipline Academic and Technical Leader Training Program of Jiangxi (Grant No. 20204BCJ23026), and the Natural Science Foundation of Jiangxi Province (Grant No. 20212BAB201018).

- 
- [1] N. Sangouard, C. Simon, H. de Riedmatten, and N. Gisin, *Rev. Mod. Phys.* **83**, 33 (2011).
- [2] C. Santori, D. Fattal, J. Vuckovic, G. S. Solomon, and Y. Yamamoto, *Nature (London)* **419**, 594 (2002).
- [3] A. Imamoglu, H. Schmidt, G. Woods, and M. Deutsch, *Phys. Rev. Lett.* **79**, 1467 (1997).
- [4] A. Verger, C. Ciuti, and I. Carusotto, *Phys. Rev. B* **73**, 193306 (2006).
- [5] A. Majumdar and D. Gerace, *Phys. Rev. B* **87**, 235319 (2013).
- [6] Y. Ren, S. H. Duan, W. Z. Xie, Y. K. Shao, and Z. L. Duan, *Phys. Rev. A* **103**, 053710 (2021).
- [7] T. C. H. Liew and V. Savona, *Phys. Rev. Lett.* **104**, 183601 (2010).
- [8] K. M. Birnbaum, A. Boca, R. Miller, A. D. Boozer, T. E. Northup, and H. J. Kimble, *Nature (London)* **436**, 87 (2005).
- [9] H. J. Sniijders, J. A. Frey, J. Norman, H. Flayac, V. Savona, A. C. Gossard, J. E. Bowers, M. P. van Exter, D. Bouwmeester, and W. Löffler, *Phys. Rev. Lett.* **121**, 043601 (2018).
- [10] C. Vaneph, A. Morvan, G. Aiello, M. Fechant, M. Aprili, J. Gabelli, and J. Esteve, *Phys. Rev. Lett.* **121**, 043602 (2018).
- [11] C. Hamsen, K. N. Tolazzi, T. Wilk, and G. Rempe, *Phys. Rev. Lett.* **118**, 133604 (2017).
- [12] S. S. Shamilov, A. S. Parkins, M. J. Collett, and H. J. Carmichael, *Opt. Commun.* **283**, 766 (2010).
- [13] A. Miranowicz, M. Paprzycka, Y. X. Liu, J. Bajer, and F. Nori, *Phys. Rev. A* **87**, 023809 (2013).
- [14] G. H. Hovsepyan, A. R. Shahinyan, and G. Y. Kryuchkyan, *Phys. Rev. A* **90**, 013839 (2014).
- [15] A. Miranowicz, J. Bajer, N. Lambert, Y. X. Liu, and F. Nori, *Phys. Rev. A* **93**, 013808 (2016).
- [16] R. Huang, A. Miranowicz, J. Q. Liao, F. Nori, and H. Jing, *Phys. Rev. Lett.* **121**, 153601 (2018).
- [17] B. Li, R. Huang, X. Xu, A. Miranowicz, and H. Jing, *Photon. Res.* **7**, 630 (2019).
- [18] Y. X. Liu, A. Miranowicz, Y. B. Gao, J. Bajer, C. P. Sun, and F. Nori, *Phys. Rev. A* **82**, 032101 (2010).
- [19] S. G. Guan, W. P. Bowen, C. J. Liu, and Z. L. Duan, *Europhys. Lett.* **119**, 58001 (2017).
- [20] M. C. Kuzyk and H. Wang, *Phys. Rev. X* **8**, 041027 (2018).
- [21] Q. Bin, X. Y. Lu, F. P. Laussy, F. Nori, and Y. Wu, *Phys. Rev. Lett.* **124**, 053601 (2020).
- [22] S. R. Sklan, *AIP Adv.* **5**, 053302 (2015).
- [23] N. Meher, *J. Phys. B: At. Mol. Opt. Phys.* **52**, 205502 (2019).
- [24] C. Zhao, R. Peng, Z. Yang, S. Chao, C. Li, and L. Zhou, *Ann. Phys.* **533**, 2100039 (2021).
- [25] K. Cai, Z. W. Pan, R. X. Wang, D. Ruan, Z. Q. Yin, and G. L. Long, *Opt. Lett.* **43**, 1163 (2018).
- [26] N. Didier, S. Pugnetti, Y. M. Blanter, and R. Fazio, *Phys. Rev. B* **84**, 054503 (2011).
- [27] T. Ramos, V. Sudhir, K. Stannigel, P. Zoller, and T. J. Kippenberg, *Phys. Rev. Lett.* **110**, 193602 (2013).
- [28] X. Wang, A. Miranowicz, H. R. Li, and F. Nori, *Phys. Rev. A* **93**, 063861 (2016).
- [29] H. Xie, C. G. Liao, X. Shang, Z. H. Chen, and X. M. Lin, *Phys. Rev. A* **98**, 023819 (2018).
- [30] J. Restrepo, I. Favero, and C. Ciuti, *Phys. Rev. A* **95**, 023832 (2017).
- [31] H. Xie, C.-G. Liao, X. Shang, M. Y. Ye, and X. M. Lin, *Phys. Rev. A* **96**, 013861 (2017).
- [32] X.-W. Xu, H.-Q. Shi, A.-X. Chen, and Y.-X. Liu, *Phys. Rev. A* **98**, 013821 (2018).
- [33] L. L. Zheng, T.-S. Yin, Q. Bin, X.-Y. Lu, and Y. Wu, *Phys. Rev. A* **99**, 013804 (2019).
- [34] J. Li, C. Ding, and Y. Wu, *J. Appl. Phys.* **128**, 234302 (2020).
- [35] T. S. Yin, Q. Bin, G. L. Zhu, G. R. Jin, and A. Chen, *Phys. Rev. A* **100**, 063840 (2019).
- [36] J. S. Tang, Y. Wu, Z. K. Wang, H. Sun, L. Tang, H. Zhang, T. Li, Y. Lu, M. Xiao, and K. Xia, *Phys. Rev. A* **101**, 053802 (2020).
- [37] Y. Wang, J. L. Wu, J. X. Han, Y. Xia, Y. Y. Jiang, and J. Song, *Phys. Rev. Appl.* **17**, 024009 (2022).
- [38] S. Barzanjeh and D. Vitali, *Phys. Rev. A* **93**, 033846 (2016).
- [39] B. Sarma and A. K. Sarma, *Phys. Rev. A* **96**, 053827 (2017).
- [40] B. Sarma and A. K. Sarma, *Sci. Rep.* **8**, 14583 (2018).
- [41] H. Q. Shi, X. T. Zhou, X. W. Xu, and N. H. Liu, *Sci. Rep.* **8**, 2212 (2018).
- [42] H. Q. Shi, Z. Q. Xie, X. W. Xu, and N. H. Liu, *Acta Phys. Sin.* **67**, 044203 (2018).
- [43] H. Li, S. Q. Zhang, M. Guo, M. X. Li, and L. J. Song, *Acta Phys. Sin.* **68**, 124203 (2019).
- [44] J.-Y. Yang, Z. Jin, J.-S. Liu, H.-F. Wang, and A. D. Zhu, *Ann. Phys.* **532**, 2000299 (2020).
- [45] C. Zhao, X. Li, S. Chao, R. Peng, C. Li, and L. Zhou, *Phys. Rev. A* **101**, 063838 (2020).
- [46] J. K. Nema, S. Gupta, R. Thakkar, and P. Rajagopal, *AIP Adv.* **11**, 015112 (2021).
- [47] L. C. Li and L. J. Liu, *J. Phys. B: At. Mol. Opt. Phys.* **54**, 055401 (2021).
- [48] M. Wang, T.-S. Yin, Z.-Y. Sun, H.-G. Cheng, B.-F. Zhan, and L.-L. Zheng, *Optics Express* **30**, 10251 (2022).
- [49] Y. X. Zeng, T. Gebremariam, J. Shen, B. Xiong, and C. Li, *Appl. Phys. Lett.* **118**, 164003 (2021).
- [50] X. W. Xu, A. X. Chen, and Y. X. Liu, *Phys. Rev. A* **94**, 063853 (2016).
- [51] H. Q. Shi, X. W. Xu, and N. H. Liu, *Sci. Rep.* **9**, 8754 (2019).
- [52] J. Tang, W. Geng, and X. Xu, *Sci. Rep.* **5**, 9252 (2015).
- [53] E. Zubizarreta Casalengua, J. C. Lopez Carreno, F. P. Laussy, and E. del Valle, *Laser Photonics Rev.* **14**, 1900279 (2020).

- [54] X. Y. Liang, Z. L. Duan, Q. Guo, S. G. Guan, M. Xie, and C. J. Liu, *Phys. Rev. A* **102**, 053713 (2020).
- [55] C. J. Zhu, K. Hou, Y. P. Yang, and L. Deng, *Photonics Res.* **9**, 1264 (2021).
- [56] R. Ohira, S. Kume, K. Takayama, S. Muralidharan, H. Takahashi, and K. Toyoda, *Phys. Rev. A* **103**, 012612 (2021).
- [57] S. Ghosh and T. C. H. Liew, *Phys. Rev. Lett.* **123**, 013602 (2019).
- [58] M. D. LaHaye, O. Buu, B. Camarota, and K. C. Schwab, *Science* **304**, 74 (2004).
- [59] K. C. Schwab and M. L. Roukes, *Phys. Today* **58**, 36 (2005).
- [60] T. Carmon, H. Rokhsari, L. Yang, T. J. Kippenberg, and K. J. Vahala, *Phys. Rev. Lett.* **94**, 223902 (2005).
- [61] M. Aspelmeyer, T. J. Kippenberg, and F. Marquardt, *Rev. Mod. Phys.* **86**, 1391 (2014).
- [62] M. Grajcar, S. Ashhab, J. R. Johansson, and F. Nori, *Phys. Rev. B* **78**, 035406 (2008).
- [63] J. B. Clark, F. Lecocq, R. W. Simmonds, J. Aumentado, and J. D. Teufel, *Nature (London)* **541**, 191 (2017).
- [64] Z. H. Peng, Y. X. Liu, J. T. Peltonen, T. Yamamoto, J. S. Tsai, and O. Astafiev, *Phys. Rev. Lett.* **115**, 223603 (2015).
- [65] S. Gasparinetti, M. Pechal, J. C. Besse, M. Mondal, C. Eichler, and A. Wallraff, *Phys. Rev. Lett.* **119**, 140504 (2017).
- [66] G. Andersson, M. K. Ekstrom, and P. Delsing, *Phys. Rev. Lett.* **124**, 240402 (2020).
- [67] M. Bamba, A. Imamoglu, I. Carusotto, and C. Ciuti, *Phys. Rev. A* **83**, 021802(R) (2011).
- [68] F. Zou, D. G. Lai, and J. Q. Liao, *Opt. Express* **28**, 16175 (2020).
- [69] J. Tang, Y. Deng, and C. Lee, *Photonics Res.* **9**, 1226 (2021).
- [70] F. Minganti, A. Miranowicz, R. W. Chhajlany, I. I. Arkhipov, and F. Nori, *Phys. Rev. A* **101**, 062112 (2020).
- [71] J. A. Mlynek, A. A. Abdumalikov, C. Eichler, and A. Wallraff, *Nat. Commun.* **5**, 5186 (2014).
- [72] A. Kowalewska-Kudłaszuk, S. I. Abo, G. Chimczak, J. Perina, F. Nori, and A. Miranowicz, *Phys. Rev. A* **100**, 053857 (2019).
- [73] C. Gardiner and P. Zoller, *Quantum Noise* (Springer-Verlag, Berlin, 2004).
- [74] M. K. Ekström, T. Aref, A. Ask, G. Andersson, B. Suri, H. Sanada, G. Johansson, and P. Delsing, *New J. Phys.* **21**, 123013 (2019).
- [75] P. Meystre and M. Sargent III, *Elements of Quantum Optics*, 4th ed. (Springer, New York, 2007).
- [76] S. Gröblacher, K. Hammerer, M. R. Vanner, and M. Aspelmeyer, *Nature (London)* **460**, 724 (2009).
- [77] X. Wang, W. Qin, A. Miranowicz, S. Savasta, and F. Nori, *Phys. Rev. A* **100**, 063827 (2019).